ACS OMEGA

Open Access

http://pubs.acs.org/journal/acsodf

Article

Improving the Separation of CO_2/N_2 Using Impregnation of a Deep Eutectic Solvent on a Porous MOF

Narmin Noorani and Abbas Mehrdad*

Cite This: *ACS Omega* 2024, 9, 9516−9525

Read Online

ACCESS | Metrics & More | Article Recommendations

ABSTRACT: As the partial pressure of CO_2 in flue gas is 0.1−0.2 bar, CO_2 capture at a low pressure needs more attention. Under low pressure conditions, the functional metal−organic framework (MOF) is powerful for CO_2 capture. One of the effective methods to increase the absorption capacity of the MOF is impregnation with deep eutectic solvents. In this research, NH_2-MIL101(Cr) is impregnated with a deep eutectic solvent of choline chloride:urea (DES ChCl:urea) to enhance the adsorption capacity. The CO_2 and N_2 adsorption capacity of NH_2-MIL101(Cr) and DES/NH_2-MIL101(Cr) was investigated at temperatures of 288.15−303.15 K and pressures up to 1 bar. The obtained results indicate that the adsorption capacity of the MOF increases by 1.7 and 3 times with the impregnated DES for CO_2 and N_2, respectively. Nevertheless, the pore volume of the MOF decreased after impregnation, but the adsorption capacity of the MOF increased due to the interaction of the adsorbate with the confined DES in pores. The contribution of the impregnated DES to adsorption capacity is explained according to Henry's law. Also, high heats of adsorption are attributed to the strong interaction between modified NH_2-MIL101(Cr) and CO_2. Also, the sample was refined at 298 K and vacuum and was reused without considerable reduction of the CO_2 capture capacity after 6 times. Moreover, the impregnation of ChCl:urea into NH_2-MIL101(Cr) nanostructures was studied using density functional theory-based approaches.

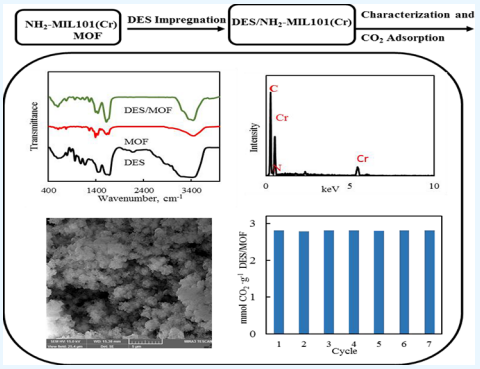

INTRODUCTION

One of the most important ecological concerns at present is related to the increase of the CO_2 concentration in the atmosphere, which arises due to fossil fuels. The CO_2 partial pressure in the flue gas varies between 0.1 and 0.2 bar with other components, especially some acidic compounds and N_2. This requires that the substance be able to continuously uptake CO_2 from postcombustion at this lower pressure.[1] Environmental problems such as ocean acidification and global warming arise due to increases of atmospheric CO_2. The majority of carbon capture technologies improved to date focus on capturing CO_2 from these considerable sources.[2] However, in order to widely use these methods, their energy use must be reduced, and their cost-effectiveness must be raised. To reduce CO_2 emissions in the energy sector, many studies have been carried out on the development of CO_2 capture and storage (CCS).[3−5] Numerous efforts have been made to develop novel CO_2 capture technologies/processes, particularly absorption based on using nanoporous solids like metal−organic frameworks, carbon materials, silica gel, carbon nanotubes, and zeolites.[6−9] These materials' special pore structures are designed to selectively inhibit CO_2 absorption and CO_2 movement in the surface of the material.[10,11]

Recently, metal−organic frameworks (MOFs) have shown good potential for CO_2 capture. MOFs have been noted as a novel category of nanoporous material. The high interior surface area, flexible porosity, tunable multifunctional pores, and good chemical and thermal stabilities support plenty of MOFs for diverse applications in gas separation.[12,13] Among the many MOFs studied so far, one of the most topical solids is the porous MIL101(Cr).[14] The MIL101(Cr) is a 3D framework due to the high pore volume, BET surface area, and high density of open metal sites. Both the open space within the porous framework and the Cr open metal sites can be impregnated with different amine species for CO_2 adsorption applications. As the CO_2 partial pressure in flue gases is 0.1−0.2 bar, CO_2 capture at this pressure range needs more attention.[15] Also, at low pressure, the BET surface area is not a significant factor for CO_2 capture. Nevertheless, the CO_2 adsorption capacity in MOFs is low, and therefore, an improvement is needed. The modification of MOFs using

Received: November 20, 2023
Revised: January 11, 2024
Accepted: February 6, 2024
Published: February 14, 2024

https://doi.org/10.1021/acsomega.3c09243
ACS Omega 2024, 9, 9516−9525

deep eutectic solvents (DESs) and ionic liquids can be performed to improve the CO_2 adsorption capacity.[16,17]

DESs have achieved growing attention as "green" alternatives to the highly expensive ionic liquid, owing to unique properties including high solvation capacity, relatively low cost, higher biodegradability, and nontoxicity making them environmentally and technologically superior.[18] Moreover, DESs due to intriguing benefits such as low volatility, low vapor pressure, and biocompatibility are favorable in many green technologies like CO_2 capture.[19] DESs are most commonly obtained by mixing a hydrogen bond donor with hydrogen bond acceptor molecules at a certain ratio. This decrease in the melting point has been related to the wide hydrogen bond network formed between different moieties in the mixture.[20] For the purpose of CO_2 capture, numerous DESs have been synthesized. The most common chemical combinations utilized in the design of DESs are mixtures of urea and choline chloride. The DES of ChCl:urea is a nontoxic, biodegradable, biocompatible, readily available, and affordable substance.[21] Li et al.[22] reported that ChCl:urea (mole ratio of 1:2) indicates the highest CO_2 solubility (0.309 mol_{CO2}/mol_{DES}) at 313 K and 12.5 MPa. Also, Leron et al.[23] found that the CO_2 solubility in ChCl:urea was higher than those of ChCl:ethylene glycol and ChCl:glycerol. However, the high viscosity of ChCl:urea needs a high pressure environment for increasing CO_2 absorption, which leads to an increase in operating costs. Furthermore, DESs and other solvents in a liquid form at ambient temperature are problematic to control.

Recently, the immobilization of DESs on porous MOFs has been attracting much attention due to the overcoming of this drawback that may lead to increased CO_2 adsorption capacity. Ariyanto et al.[19] studied DES-impregnated porous carbon for the CH_4/CO_2 separation. DESs of choline chloride:alcohols impregnated on the porous carbon were derived from the palm kernel shell (C-PKS). Lin et al.[24] also investigated CO_2 capture in a DES (ChCl:ethylene glycol) confined into graphene oxide (GO) with different molar ratios of HBA/HBD by molecular dynamics simulations, i.e., GO makes available confined space for the DES, consequently the special spatial configuration, and also the DES-GO interaction. Also, the interaction between DES molecules weakened, which increases the free volume and results in the diffusion of gas. Ghazali et al.[25] found that the modification of mesoporous silica gel (SG) with impregnation of ChCl:urea can be considered as a promising adsorbent for CO_2 capture at atmospheric pressure and ambient temperature. However, the data of the isotherm of the NH_2-MIL101(Cr) impregnated with the DES for the separation process are scarce. In this research, a choline chloride:urea (1:2) DES was prepared and impregnated to NH_2-MIL101-(Cr) for CO_2 adsorption. The CO_2 adsorption in the DES/NH_2-MIL101(Cr) was determined by a quartz crystal microbalance (QCM) at temperatures of 288.15 and 303.15 K. The adsorption isotherm to study the potential of the material for separation purposes was investigated. A new hybrid model has been proposed to correlate the CO_2 adsorption isotherm. In addition, the CO_2/N_2 selectivity was carried out to examine the practical efficacy of the prepared adsorbents.

2. EXPERIMENTAL SECTION

2.1. Materials. Chromium nitrate nonahydrate ($Cr(NO_3)_3 \cdot 9H_2O$) (>99% purity), 2-aminoterephthalic acid (NH_2-H_2BDC, ≥99% purity), and choline chloride (>99% purity) were purchased from Sigma-Aldrich. *N*,*N*-Dimethylformamide (DMF) (>99% purity), urea (>99% purity), sodium hydroxide (NaOH), and ethanol (>99% purity) were supplied by Merck. CO_2 gas (>99.9% purity) was used in gas absorption tests.

2.2. Synthesis of NH_2-MIL101(Cr). NH_2-MIL101(Cr) was synthesized by using the hydrothermal technique. To synthesize NH_2-MIL101(Cr), 1.6 g of chromium nitrate nonahydrate ($Cr(NO_3)_3 \cdot 9H_2O$), 0.72 g of 2-aminoterephthalic acid (NH_2-H_2BDC), 0.4 g of NaOH, and 30 mL of deionized water were combined in a Teflon-lined autoclave. The homogeneous solution was heated in an autoclave in a particular Teflon container for 8 h at 423 K. Then, the slurry was centrifuged. The green product obtained was washed with DMF, deionized water, and ethanol to eliminate the unreacted chemicals in the pores. Then, the synthesized NH_2-MIL101-(Cr) became dry at 373 K for about 12 h under vacuum.

2.3. Synthesis of the DES. In this work, a ChCl:urea (1:2 mol ratio) DES was obtained by mixing choline chloride and urea under stirring at 360 K for about 2 h. Then, the obtained homogeneous solution was cooled to ambient temperature and is liquid, homogeneous, viscous, and colorless at ambient temperature, and its melting point was below room temperature. The melting point of ChCl/urea is 285 K, which is in good agreement with the literature.[26]

2.4. Synthesis of DES Confinement in NH_2-MIL101-(Cr). NH_2-MIL101(Cr) was impregnated by ChCl/urea (1:2) using a vacuum impregnation method. The product was dried at 378 K for 20 h.

2.5. Characterization of the MOF. The morphology of NH_2-MIL101(Cr) was studied by providing FESEM images (EDX, map and line). To distinguish the Cr of the MOF, EDX spectra were recorded in the same microscope working at 10 keV. The samples were degassed in vacuum at 120 °C for 10 h before measurement. The BET surface area of the NH_2-MIL101(Cr) and DES/NH_2-MIL101(Cr) was also obtained by measuring the nitrogen adsorption at 77 K using a BELSORP MINI II instrument. Also, the FTIR spectra of NH_2-MIL101(Cr) and DES/NH_2-MIL101(Cr) were recorded using a spectrometer (Bruker, Tensor 27).

2.6. Gas Adsorption Apparatus. For the purpose of measuring gas adsorption, a QCM sensor was applied. The adsorption apparatus performance has been discussed in the previous works by authors in detail.[27−31] The adsorbent adsorption capacity, Q_e ($mmol_{CO_2} \cdot g^{-1}_{MOF}$) was calculated as follows:

$$Q_e = \frac{\Delta F_S}{\Delta F_C} \times \frac{1000}{44} \quad (1)$$

where ΔF_C is the difference in frequencies between uncoated and coated crystals with the adsorbent. ΔF_S is the difference in frequency between DES/NH_2-MIL101(Cr)-coated crystals under vacuum and after gas adsorption.

2.7. Thermodynamic Model. The three-parameter Redlich−Peterson (R−P) model was used to fit the experimental isotherms in the MOF as follows:[32]

$$Q_e = q_m \frac{cp}{1 + cp^n} \quad (2)$$

where p indicates gas pressure in equilibrium conditions, n is the dimensionless parameter that was assumed as $n = 1$ in this work, and c and q_m are R−P model's parameters. A hybrid R−P

https://doi.org/10.1021/acsomega.3c09243
ACS Omega 2024, 9, 9516−9525

and Henry's law model was used to correlate the experimental adsorption data in DES/NH_2-MIL101(Cr) as follows:

$$Q_e = \frac{p}{H} + q_m \frac{cp}{1 + cp^n} \quad (3)$$

where H is Henry's law constant. The adsorption selectivity for CO_2/N_2 was calculated as follows:

$$S_{CO_2/N_2} = \frac{Q_{CO_2}}{Q_{N_2}} \quad (4)$$

where Q_{CO_2} and Q_{N_2} are the absolute adsorbed values of CO_2 and N_2, respectively.

3. RESULTS AND DISCUSSION

3.1. Characterization. *3.1.1. FTIR Spectra.* The FTIR spectra of the choline chloride-urea DES, NH_2-MIL101(Cr), and DES-impregnated NH_2-MIL101(Cr) are represented in Figure 1. As seen from Figure 1a, the spectra of the DES

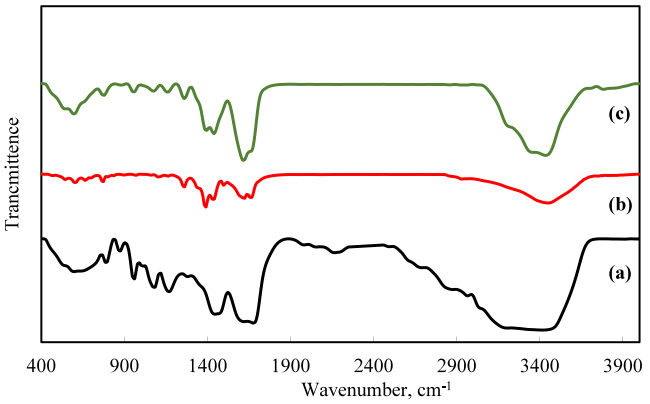

Figure 1. FTIR spectra of the synthesized (a) DES, (b) NH_2-MIL101(Cr), and (c) the DES/NH_2-MIL101(Cr).

indicate a broad band at ~3400 cm^{-1}, which corresponds to the hydrogen-bonded hydroxyl functional group between urea and choline.[33,34] The existence of the carboxylate linker in NH_2-MIL101(Cr) was shown by the presence of bands in 1300−1750 cm^{-1}, which are related to the COO symmetric and asymmetric stretching vibrations and the stretching vibrations of C−C. The weak signal at 960 cm^{-1} and the sharp signal at 760 cm^{-1} were attributed to C−H of the aromatic ring out-of-plane and in-plane bending vibration, respectively (Figure 1b).[35] Also, analysis of FTIR peaks in Figure 1c reveals the bands at 3450 and 3500 cm^{-1}, which are related to the symmetric and asymmetric stretching vibration of N−H in the amino groups, respectively.[36] Also, the obvious bands in the region of 1660−1380 cm^{-1} are attributed to the COO^- symmetric vibration, C−C stretching vibration, and asymmetric stretching vibration, indicating the NH_2-MIL101-(Cr) carboxylate linker. The peaks at 1660 and 1582 cm^{-1} are attributed to the asymmetric CO_2 stretching mode of carboxylic groups. In addition, analysis of FTIR peaks in Figure 1c reveals that the bands at 3370 and 3430 cm^{-1} are related to the asymmetric and symmetric stretching of primary amines, which shows the presence of amino groups; moreover, another band at 596 cm^{-1} agrees with previous observations for NH_2-MIL101(Cr).

3.1.2. EDX Spectroscopy Pattern. EDX spectroscopy was used to evaluate the elemental distribution in the NH_2-MIL101(Cr). Figure 2 shows the pattern that corresponds to

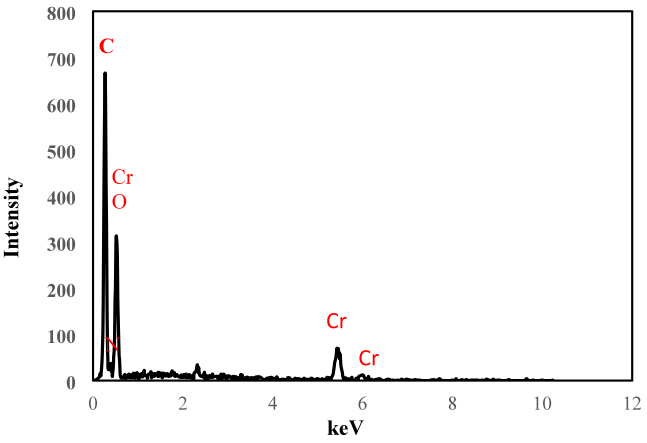

Figure 2. EDX pattern of synthesized NH_2-MIL101(Cr).

the distinctive components of NH_2-MIL101(Cr). EDX confirmed elements of chrome, carbon, nitrogen, and oxygen in the structure of NH_2-MIL101(Cr). Based on the results of the characteristic elements, the mass fractions of C and N are 47.68 and 8.21%, respectively. Therefore, molar ratio of C to N is equal to 5.81, which is close to the molar ratio of C to N in the NH_2-H_2BDC molecule. These outcomes demonstrate the purity of synthesized NH_2-MIL101(Cr).

3.1.3. Scanning Electron Microscopy. The morphology of the samples' structures is investigated using SEM. Scanning electron microscopy (SEM) images of the NH_2-MIL101(Cr) are depicted in Figure 3. The morphology and topology of the NH_2-MIL101(Cr) were confirmed to be a quasi-cubic structure.

3.1.4. Textural Properties of NH_2-MIL101(Cr). The textural characteristics of the DES/NH_2-MIL101(Cr) such as the specific surface area (A_{BET}), total pore volume (V_P), and mean pore diameter (D_{MP}) were measured using the N_2 adsorption/desorption isotherms. As depicted in Figure 4, as typical of microporous crystalline materials, type IV isotherms were obtained.[37] The surface areas of the samples were obtained by the BET method based on N_2 adsorption/desorption isotherms. The total pore volumes were determined from the N_2 adsorption volume at p/p_0 = 0.991. Observation of hysteresis loops for NH_2-MIL101(Cr) implies that NH_2-MIL101(Cr) is mesoporous. The textural properties of NH_2-MIL101(Cr) and DES/NH_2-MIL101(Cr) are reported in Table 1, which are consistent with the values reported in the literature.[38,39] Textural properties show that the impregnation procedure reduces the specific surface area, total pore volume, and micropore volume compared to the original NH_2-MIL101(Cr) sample. The obvious decrease in the pore volume as well as the surface area indicated that the NH_2-MIL101(Cr) pores were occupied by the bulky DES. The adsorbed nitrogen over NH_2-MIL101(Cr) impregnated with DESs was comparably low, probably because of partial filling or blocking of the pores of NH_2-MIL101(Cr) with an excess of DES species. This behavior may be due to the DES located near the pore opening of NH_2-MIL101(Cr) or inside the porous framework.

https://doi.org/10.1021/acsomega.3c09243
ACS Omega 2024, 9, 9516−9525

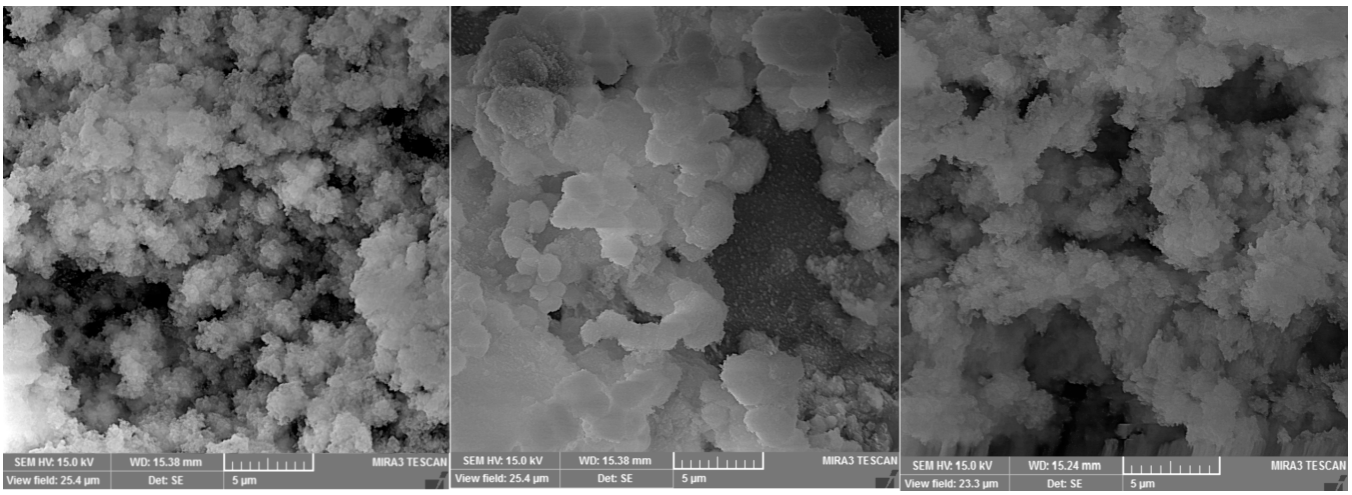

Figure 3. SEM images of synthesized NH_2-MIL101(Cr).

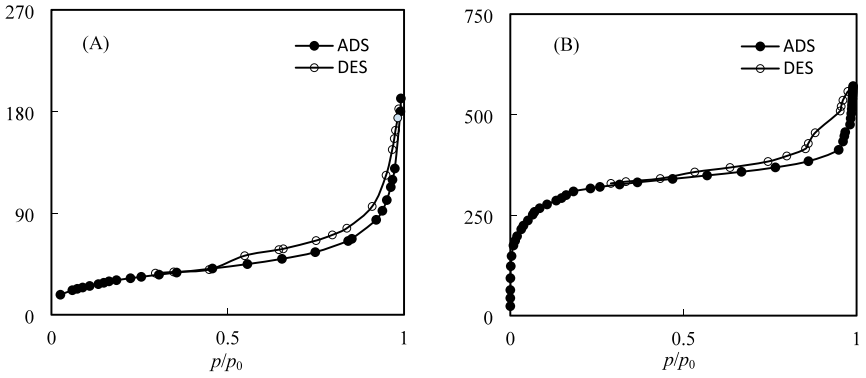

Figure 4. Nitrogen desorption/adsorption isotherms at 77 K: (A) NH_2-MIL101(Cr) and (B) DES/NH_2-MIL101(Cr).

Table 1. Textural Characteristics of the Samples

adsorbent	A_{BET} ($m^2 \cdot g^{-1}$)	V_P ($cm^3 \cdot g^{-1}$)	D_{MP} (nm)
NH_2-MIL101(Cr)	1073.1	0.882	3.29
DES/NH_2-MIL101(Cr)	115.47	0.284	9.83

3.2. Adsorption Isotherms. CO_2 and N_2 gas adsorption in NH_2-MIL101(Cr) and DES/NH_2-MIL101(Cr) was measured at a pressure of up to 1 bar and temperatures of 288.15−303.15 K. The CO_2 and N_2 gas adsorption data are listed in Tables 2 and 3. The gas adsorption capacities of NH_2-MIL101(Cr) and DES/NH_2-MIL101(Cr) are fitted using the P−R and hybrid model, respectively. The calculated parameters of these models for CO_2 and N_2 adsorption in NH_2-MIL101(Cr) and DES/NH_2-MIL101(Cr) along with the absolute average relative deviation (AARD) are reported in Tables 4 and 5. The reported AARD indicates that the capability of the proposed model was suitable. As seen from Tables 2 and 3, the impregnation of the DES into NH_2-MIL101(Cr) can make novel stronger adsorption sites and improves the CO_2 adsorption capacity. Compared to this pure DES,[40] the DES/NH_2-MIL101(Cr) owned higher CO_2 capture, which is attributed to both chemical and physical adsorption. Also, the increase of CO_2 capture on DES/NH_2-MIL101(Cr) compared to NH_2-MIL101(Cr) at 298 K and 0.15 bar, which corresponds to the pressure of CO_2 in flue gases, was 16.8%. This behavior can be attributed to the interaction between guest CO_2 molecules and amine of the DES. The $-NH_2$ groups and CO_2 can be chemically combined with a molar fraction of 2:1 ($-NH_2$:CO_2) due to forming carbamate. Subsequently, sites of the $-NH_2$ adsorption were entirely occupied, and CO_2 can interact more strongly with the −OH group of choline chloride. During the adsorption process, sites of the open metal would also be advantageous for the CO_2 uptake.

The BET surface area and pore volume of the DES/NH_2-MIL101(Cr) decreased with a further increase of the incorporated DES into NH_2-MIL101(Cr). This behavior implies a further decrease in the BET surface area through porosity blockage resulting from the added DES. The isotherm curves of the CO_2 and N_2 gas adsorption of the considered systems at different temperatures and pressures are illustrated in Figure 5. As mentioned, NH_2-MIL101(Cr) impregnated with the DES not only reduced the surface area and pore volume but also modified the surface chemistry owing to the presence of numerous $-NH_2$ groups. Hence, the rise of the CO_2 adsorption capacity in DES/NH_2-MIL101(Cr) is attributed to the production of more adsorptive sites on the adsorbent. The improved CO_2 adsorption performance on NH_2-MIL101(Cr) is attributed to the incorporation of the DES into NH_2-MIL101(Cr), which leads to CO_2 approaching to extra active sites on the pore surface, interaction between $-NH_2$ and −OH groups, clogging of porosity, and reduction of the BET surface area. According to Figure 5, NH_2-MIL101(Cr) has a CO_2 adsorption capacity of 2.189 $mmol_{CO_2} \cdot g^{-1}_{MOF}$, while DES/$NH_2$-MIL101(Cr) has an

https://doi.org/10.1021/acsomega.3c09243
ACS Omega 2024, 9, 9516−9525

Table 2. CO_2 Adsorption Capacity Q_e ($mmol_{CO_2} \cdot g^{-1}_{MOF}$) of NH_2-MIL101(Cr) and DES/NH_2-MIL101(Cr) at the 288.15–303.15 K Temperature Range and Pressures up to 1 bar[a]

T = 288.15 K		T = 293.15 K		T = 298.15 K		T = 303.15 K	
p/bar	$Q_e/mmol_{CO_2} \cdot g^{-1}_{MOF}$	p/bar	$Q_e/mmol_{CO_2} \cdot g^{-1}_{MOF}$	p/bar	$Q_e/mmol_{CO_2} \cdot g^{-1}_{MOF}$	p/bar	$Q_e/mmol_{CO_2} \cdot g^{-1}_{MOF}$
NH_2-MIL101(Cr)							
0.151	0.576	0.157	0.521	0.15	0.434	0.153	0.421
0.283	1.040	0.258	0.788	0.263	0.698	0.275	0.707
0.346	1.234	0.310	0.882	0.337	0.892	0.313	0.809
0.487	1.587	0.487	1.345	0.412	1.054	0.387	0.942
0.51	1.664	0.534	1.478	0.487	1.217	0.496	1.164
0.624	1.900	0.607	1.614	0.528	1.351	0.538	1.234
0.703	2.084	0.723	1.8261	0.64	1.555	0.678	1.425
0.787	2.236	0.787	1.945	0.787	1.821	0.739	1.537
0.823	2.34	0.856	2.106	0.844	1.925	0.862	1.682
0.921	2.490	0.923	2.204	0.921	2.080	0.937	1.765
1.011	2.620	1.003	2.320	1.002	2.189	1.006	1.854
DES/NH_2-MIL101(Cr)							
0.153	0.851	0.151	0.783	0.158	0.729	0.157	0.617
0.229	1.242	0.256	1.242	0.223	0.943	0.215	0.773
0.345	1.772	0.348	1.615	0.345	1.511	0.392	1.253
0.425	2.089	0.431	1.915	0.433	1.799	0.487	1.511
0.565	2.642	0.542	2.318	0.523	2.093	0.579	1.760
0.618	2.851	0.613	2.575	0.601	2.349	0.678	2.029
0.717	3.242	0.787	3.208	0.796	2.985	0.784	2.238
0.816	3.618	0.854	3.450	0.884	3.275	0.887	2.509
0.966	4.225	0.923	3.701	0.978	3.583	0.981	2.736
1.004	4.376	1.008	3.978	1.010	3.688	1.014	2.782

[a]Standard uncertainties are $u(Q_e) = 0.001$, $u(T) = 0.05$ K, and $u(p) = 0.001$.

Table 3. N_2 Adsorption Capacity Q_e ($mmol_{CO_2} \cdot g^{-1}_{MOF}$) of NH_2-MIL101(Cr) and DES/NH_2-MIL101(Cr) at the 288.15–303.15 K Temperature Range and Pressures up to 1 bar[a]

T = 288.15 K		T = 293.15 K		T = 298.15 K		T = 303.15 K	
p/bar	$Q_e/mmol_{N_2} \cdot g^{-1}_{MOF}$	p/bar	$Q_e/mmol_{N_2} \cdot g^{-1}_{MOF}$	p/bar	$Q_e/mmol_{N_2} \cdot g^{-1}_{MOF}$	p/bar	$Q_e/mmol_{N_2} \cdot g^{-1}_{MOF}$
NH_2-MIL101(Cr)							
0.152	0.0667	0.157	0.0598	0.156	0.0489	0.159	0.0423
0.220	0.094	0.275	0.092	0.221	0.067	0.283	0.076
0.367	0.148	0.313	0.113	0.359	0.110	0.321	0.084
0.450	0.180	0.427	0.155	0.421	0.132	0.42	0.111
0.574	0.228	0.516	0.188	0.523	0.162	0.590	0.154
0.628	0.245	0.615	0.220	0.615	0.195	0.623	0.163
0.705	0.272	0.703	0.247	0.716	0.219	0.695	0.181
0.804	0.302	0.787	0.275	0.805	0.249	0.769	0.200
0.887	0.325	0.897	0.310	0.876	0.272	0.818	0.210
0.978	0.350	0.978	0.334	0.945	0.292	0.904	0.234
1.002	0.357	1.005	0.342	1.001	0.310	1.004	0.252
DES/NH_2-MIL101(Cr)							
0.151	0.264	0.153	0.244	0.158	0.244	0.151	0.176
0.237	0.367	0.238	0.333	0.256	0.335	0.229	0.241
0.337	0.484	0.329	0.438	0.347	0.440	0.384	0.371
0.415	0.569	0.477	0.593	0.433	0.520	0.475	0.446
0.516	0.677	0.564	0.684	0.547	0.627	0.583	0.536
0.609	0.791	0.628	0.751	0.635	0.709	0.678	0.616
0.782	0.974	0.739	0.867	0.737	0.804	0.768	0.691
0.877	1.066	0.811	0.942	0.846	0.905	0.845	0.755
0.976	1.173	0.900	1.036	0.963	1.014	0.920	0.817
1.005	1.204	1.005	1.145	1.010	1.058	1.004	0.887

[a]Standard uncertainties are $u(Q_e) = 0.001$, $u(T) = 0.05$ K, and $u(p) = 0.001$.

https://doi.org/10.1021/acsomega.3c09243
ACS Omega 2024, 9, 9516−9525

Table 4. Henry's Law Constant (H), q_m, and c That Are Also Parameters of the Redlich–Peterson Isotherm Model, the Correlation Coefficient (R^2), and Absolute Average Relative Deviation (AARD) for CO_2 Adsorption on NH_2-MIL101(Cr) and DES/NH_2-MIL101(Cr) at Different Temperatures (T)[a]

adsorbent	T/K[aa]	H/bar	q_m/mmol$_{CO_2}$·g$^{-1}_{MOF}$	c/bar^{-1}	[b]AARD%
NH_2-MIL101(Cr)	288.15		6.601	0.656	0.67
	293.15		8.400	0.458	1.09
	298.15		8.396	0.354	0.78
	303.15		4.540	0.684	0.75
DES/NH_2-MIL101(Cr)	288.15	0.269	0.781	4.210	1.50
	293.15	0.294	0.678	4.577	0.27
	298.15	0.363	1.459	1.563	0.86
	303.15	0.442	0.627	4.111	0.72

[a]The standard uncertainty is $u(T) = 0.05$ K. [b]AARD% $= \frac{100}{n}\sum\left|\frac{Q_{CO_2}^{cal} - Q_{CO_2}^{exp}}{Q_{CO_2}^{exp}}\right|$.

Table 5. Henry's Law Constant (H), q_m, and c That Are Also Parameters of the Redlich–Peterson Isotherm Model, the Correlation Coefficient (R^2), and Absolute Average Relative Deviation (AARD) for N_2 Adsorption on NH_2-MIL101(Cr) and DES/NH_2-MIL101(Cr) at Different Temperatures (T)[a]

adsorbent	T/K[a]	H/bar	q_m/mmol$_{N_2}$·g$^{-1}_{MOF}$	c/bar^{-1}	[b]AARD%
NH_2-MIL101(Cr)	288.15		1.685	0.270	0.61
	293.15		3.759	0.100	1.27
	298.15		3.768	0.060	0.72
	303.15		3.515	0.070	0.59
DES/NH_2-MIL101(Cr)	288.15	0.957	0.169	10.561	0.19
	293.15	0.962	0.104	26.294	0.33
	298.15	1.094	0.145	12.460	0.43
	303.15	1.237	0.090	5.445	0.57

[a]The standard uncertainty is $u(T) = 0.05$ K. [b]AARD% $= \frac{100}{n}\sum\left|\frac{Q_{N_2}^{cal} - Q_{N_2}^{exp}}{Q_{N_2}^{exp}}\right|$.

adsorption capacity of 3.688 mmol$_{CO_2}$·g$^{-1}_{DES/MOF}$ at a temperature of 298.15 K and a pressure of 1 bar. The reported CO_2 adsorption capacity value in the literature for nonamine-functionalized MIL101(Cr) at 298.15 K and a pressure of 1 bar is 1.6 mmol$_{CO_2}$·g$^{-1}_{MOF}$.[41] Therefore, the amine-functionalized MIL101(Cr) has a higher adsorption capacity than nonamine-functionalized MIL101(Cr). Also, Lawson et al.[41] have achieved adsorption capacities of 2 and 3.6mmol$_{CO_2}$·g$^{-1}_{MOF}$ by impregnation of polyethylenimine and tetraethylenepentamine into MIL101(Cr) at 298.15 K and a pressure of 1 bar. This behavior implies the presence of amine groups in NH_2-MIL101(Cr) owing to the fact that the Lewis basic amine groups can interact strongly with the CO_2 molecules. Moreover, the quadrupole moment of CO_2 (-14×10^{-40} C m^2) is much higher than that of N_2 (-4.6×10^{-40} C m^2) that leads to the higher capture of CO_2 than that of N_2. Also, in the DES-impregnated MOF, gas adsorption can be due to two factors; the first factor is confinement of the DES in pores of the MOF, and the second factor is immobilization of the DES on the pore surface. At a low pressure, gas adsorption occurred on the immobilized DES on the pore surface of NH_2-MIL101(Cr), while at a high pressure, gas adsorption happened on the confined DES in MIL101(Cr) pores. In addition, the chemical reaction between the amine group and CO_2 molecules affects the CO_2 adsorption in NH_2-MIL101-(Cr). The several active sites in NH_2-MIL101(Cr) such as the NH_2 functional group and carboxylate oxygen atoms can increase preferential interactions between CO_2 and the MOF.

The selectivity of CO_2/N_2 for NH_2-MIL101(Cr) and DES/NH_2-MIL101(Cr) was evaluated at a temperature of 288.15 K and different pressures. The selectivities of CO_2/N_2 for NH_2-MIL101(Cr) and DES/NH_2-MIL101(Cr) are illustrated in Figure 6. The CO_2 adsorption in the bare amine-functionalized MOF often is chemisorption, but N_2 adsorption in the bare amine-functionalized MOF is physisorption. However, in the DES/MOF, moreover, surface adsorption on one portion of adsorption is related to the physical absorption in the confined DES in the pores of the MOF, which is governed by Henry's law. Therefore, the selectivity of the bare amine-functionalized MOF is higher than that of the DES/MOF. The value of CO_2/N_2 selectivity decreases with an increase in the pressure and tends to plateau, which is in good agreement with the literature.[42]

3.3. Enthalpy of Adsorption. The molar enthalpy of adsorption is a measure of the strength of interaction between the adsorbate molecules and the adsorbent surface, which can be calculated by measuring gas adsorption at various temperatures.[43,44] The isotropic heat adsorption at a constant adsorption amount, q, was calculated as follows:[45,46]

$$\Delta H_s = R\left(\frac{\partial \ln p}{\partial(1/T)}\right)_q = RT^2\left(\frac{\partial \ln p}{\partial T}\right)_q \quad (5)$$

where R is the universal gas constant and T is temperature. In order to calculate the heat of absorption, absorption experiments were performed at temperatures of 303.15–288.15 K. The influence of temperature on the absorption of CO_2 by DES/NH_2-MIL101(Cr) adsorbents is shown in Figure 5. According to Figure 5, the adsorption isotherm is temperature-

https://doi.org/10.1021/acsomega.3c09243
ACS Omega 2024, 9, 9516–9525

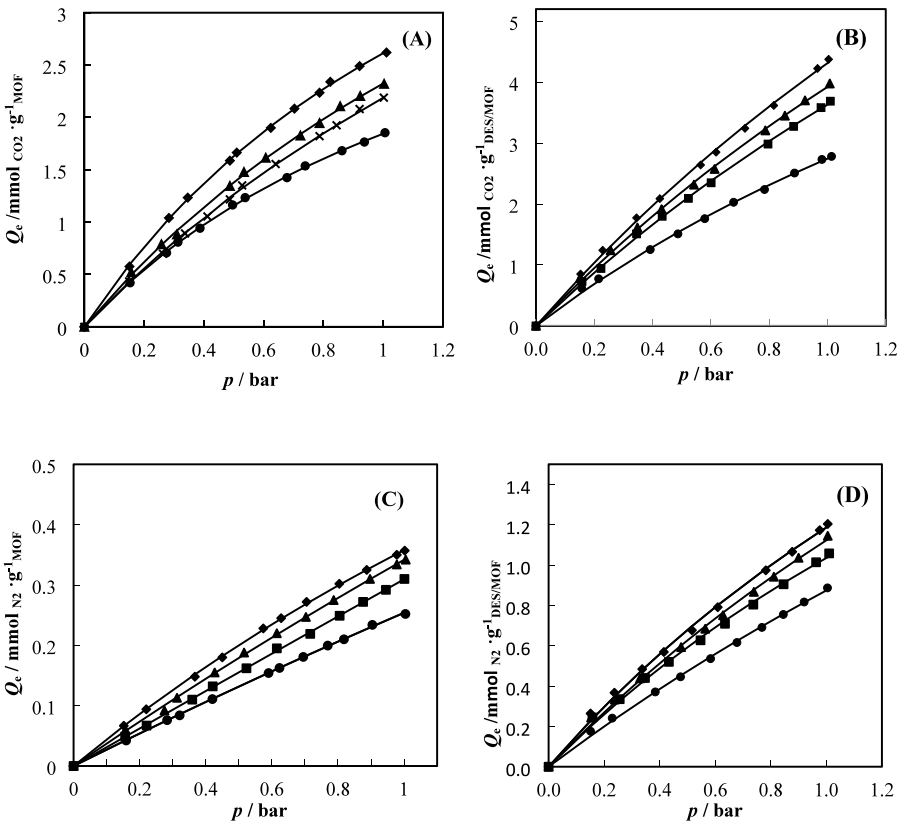

Figure 5. CO_2 adsorption in (A) NH_2-MIL101(Cr) and (B) DES/NH_2-MIL101(Cr) and N_2 adsorption in (C) NH_2-MIL101(Cr) and (D) DES/NH_2-MIL101(Cr) at different temperatures (diamonds) 288.15K; (triangles) 293.15 K; (square) 298.15 K; (circles) 303.15 K; (lines) fitting results by eq 3.

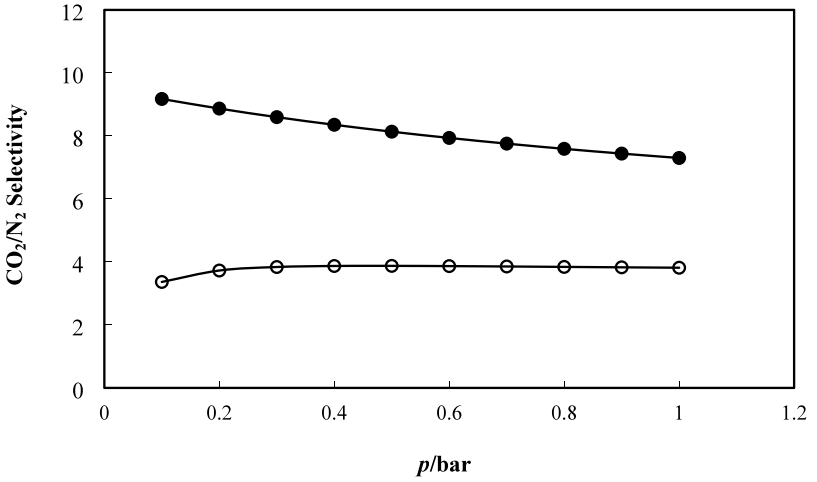

Figure 6. Selectivity of CO_2/N_2 based on the ratio of adsorption uptake at 288.15 K for (filled circles) NH_2-MIL101(Cr) and (open circles) DES/NH_2-MIL101(Cr).

dependent. The isosteric heat values for NH_2-MIL101(Cr) and DES/NH_2MIL101(Cr) are obtained from plotting ln(P) vs 1/T. The obtained isosteric heat versus adsorption capacity is illustrated in Figure 7. According to Figure 7, isosteric heat of adsorption is decreased with increasing adsorption. Gas absorption in the confined DES in the pores of the MOF is physical sorption, which is governed by Henry's law. The heat of physical adsorption is lower than that of chemical sorption; therefore, a higher adsorption heat in the amine-functionalized MOF than in the DES/MOF is expected.

3.4. Regeneration Efficiency. To evaluate the reusability of the adsorbent, an adsorption/desorption process was performed for up to seven cycles. For regeneration tests, CO_2 absorption was tested at 298.15 K and 1 bar, and vacuum and desorption processes were done at vacuum and 298.15 K up to 90 min for CO_2 elimination. The regeneration capability of the DES/NH_2-MIL101(Cr) adsorbent in seven cycles is shown in Figure 8. As shown in Figure 8, the amount of adsorbed CO_2 was slightly reduced after seven cycles. The amounts of CO_2 adsorption in DES/NH_2-MIL101(Cr) are obtained to be 2.817, 2.817, 2.817, 2.817, 2.809, 2.809, and

https://doi.org/10.1021/acsomega.3c09243
ACS Omega 2024, 9, 9516−9525

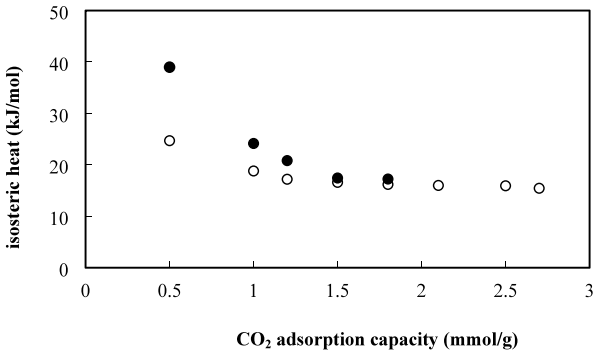

Figure 7. Isosteric heat of CO_2 adsorption on (filled circles) NH_2-MIL101(Cr) and (open circles) DES/NH_2-MIL101(Cr).

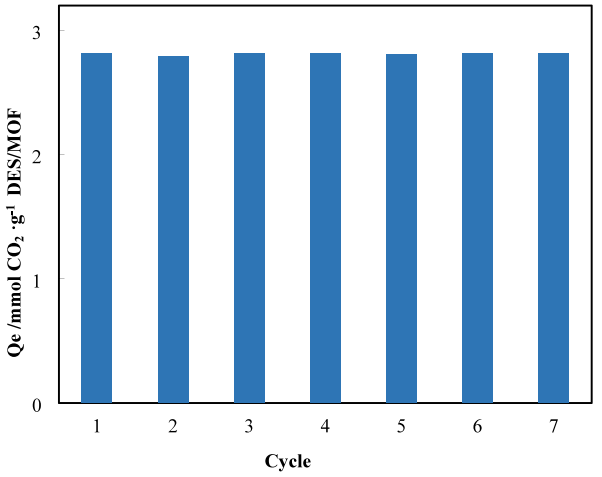

Figure 8. CO_2 absorption capacity of DES/NH_2-MIL101(Cr) at p = 1.000 bar and T = 298.15 K in seven adsorption/desorption cycles.

2.809 in seven repeated cycles of adsorption/desorption, and the regeneration performance of DES/NH_2-MIL101(Cr) is 99.7% after seven consecutive cycles of adsorption/desorption.

3.5. DFT Calculations. The study of the CO_2 adsorption mechanism in the ChCl:urea-incorporated NH_2-MIL101(Cr) complex has been carried out at the molecular level. In order to find the structural properties and stability of ChCl/urea that was incorporated into NH_2-MIL101(Cr) pores, the different structures of the pure ChCl:urea DES, NH_2-MIL101(Cr) structure, and ChCl:urea-incorporated NH_2-MIL101(Cr) complex were optimized at the B3LYP-D3/6-311G*(d,p) level of DFT theory as realized in the Gaussian 03 computational package.[47−49] The most stable configurations were used to study CO_2 adsorption. The adsorption energy (E_{ads}) was obtained using the following equation:[50]

$$E_{ads} = EE_{tot}(\text{DES/NH}_2\text{-MIL101} + CO_2) - E_{tot}(\text{NH}_2\text{-MIL101}) - E_{tot}(\text{DES}) - E_{tot}(CO_2) \quad (6)$$

To obtain the most probable sites of the interactions between the ChCl/urea and ChCl/urea confinement in NH_2-MIL101(Cr), different several structures of ChCl/urea and NH_2-MIL101(Cr) were considered based on the partial charge distribution and the full optimization of structures, and their energies were calculated. The interaction energy of ChCl/urea-impregnated NH_2-MIL101(Cr) is −112 kcal·mol^{-1}. The geometries of the selected ChCl/urea, NH_2-MIL101(Cr) structure, and ChCl/urea-impregnated NH_2-MIL101(Cr) complex are shown in Figure 9. This approach enables an obvious picture of the microscopic interfacial interaction between ChCl/urea and NH_2-MIL101(Cr). In addition, the degree of stability was based on the nature of surface charge transfer in the complex. The optimized geometries along with the shortest interaction distances between ChCl/urea and the NH_2-MIL101(Cr) framework are shown in Figure 9. ChCl/urea geometries of the DES are not altered even in the confined environment and stabilized by the electrostatic interactions and H-bonds. The calculated interacting distance of ChCl/urea−surface was varied from 2.13 to 2.67 Å. This phenomenon implies that Cl strongly interacts with the surface that notably increases the calculated adsorption energies and causes the increase of the volume of the NH_2-MIL101(Cr) structure.

4. CONCLUSIONS

The potential of DES-impregnated NH_2-MIL101(Cr) was assessed for the separation of CO_2/N_2. Choline chloride was used in conjunction with urea, which was used to modify amino-functionalized NH_2-MIL101(Cr). BET, SEM-EDX, and FTIR analysis confirmed that the DES is impregnated into the porous MOF. CO_2/N_2 adsorption isotherms revealed that DES/NH_2-MIL101(Cr) exhibited a better performance. The results show that in addition to physical adsorption, the chemical adsorption of CO_2 by the functional group of NH_2 in

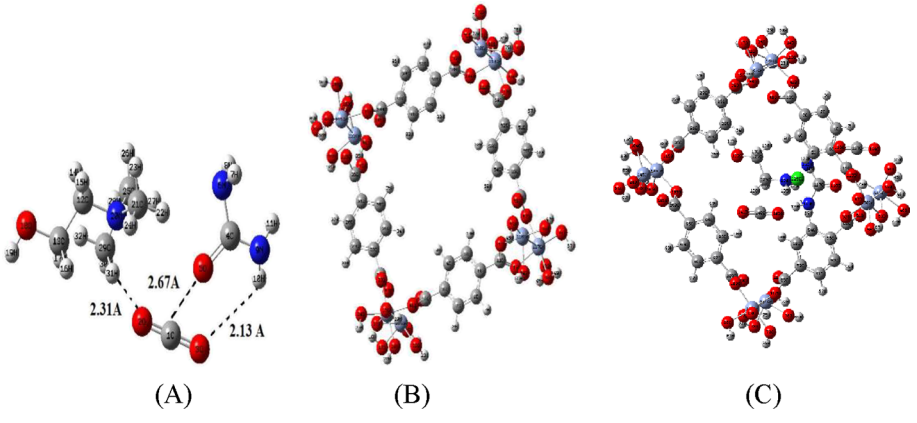

Figure 9. Structures of (A) DES with CO_2 (B) NH_2-MIL101(Cr) and (C) DES/NH_2-MIL101(Cr) with CO_2.

https://doi.org/10.1021/acsomega.3c09243
ACS Omega 2024, 9, 9516−9525

the structure of the adsorbent also has a significant effect on the adsorption mechanism. The DES/NH_2-MIL101(Cr) can be employed repeatedly without losing adsorption performance and could increase the CO_2 uptake capacity, which introduces a new class of extremely porous adsorbents for effective absorption.

AUTHOR INFORMATION

Corresponding Author

Abbas Mehrdad − *Department of Physical Chemistry, Faculty of Chemistry, University of Tabriz, Tabriz 51666, Iran;* orcid.org/0000-0002-1181-3512; Email: a_mehrdad@tabrizu.ac.ir

Author

Narmin Noorani − *Department of Physical Chemistry, Faculty of Chemistry, University of Tabriz, Tabriz 51666, Iran;* orcid.org/0000-0002-8156-2018

Complete contact information is available at: https://pubs.acs.org/10.1021/acsomega.3c09243

Notes

The authors declare no competing financial interest.

ACKNOWLEDGMENTS

The authors are thankful for the postdoctoral grant (no. SAD/3938-1400 1225) from the University of Tabriz.

REFERENCES

(1) Wang, W.; Wang, S.; Ma, X.; Gong, J. Recent Advances in Catalytic Hydrogenation of Carbon Dioxide. *Chem. Soc. Rev.* **2011**, *40*, 3703−3727.

(2) Li, W.; Wang, H.; Jiang, X.; Zhu, J.; Liu, Z.; Guo, X.; Song, C. A. Short Review of Recent Advances in CO_2 Hydrogenation to Hydrocarbons over Heterogeneous Catalysts. *RSC Adv.* **2018**, *8*, 7651−7669.

(3) Yin, F.; Zhuang, L.; Luo, X.; Chen, S. Simple synthesis of nitrogen-rich polymer network and its further amination with PEI for CO_2 adsorption. *Appl. Surf. Sci.* **2018**, *434*, 514−521.

(4) Chen, C.; Li, B.; Zhou, L.; Xia, Z.; Feng, N.; Ding, J.; Wang, L.; Wan, H.; Guan, G. Synthesis of hierarchically structured hybrid materials by controlled self-assembly of metalorganic framework with mesoporous silica for CO_2 adsorption. *Acs Appl. Mater. Inter.* **2017**, *9*, 23060−23071.

(5) Zhang, S. H.; Shen, Y.; Shao, P. J.; Chen, J. M.; Wang, L. D. Kinetics, thermodynamics, and mechanism of a novel biphasic solvent for CO_2 capture from flue gas. *Environ. Sci. Technol.* **2018**, *52*, 3660−3668.

(6) Barzagli, F.; Mani, F.; Peruzzini, M. A ^{13}C NMR study of the carbon dioxide absorption and desorption equilibria by aqueous 2-aminoethanol and Nmethylsubstituted 2-aminoethanol. *Energy Environ. Sci.* **2009**, *2*, 322−330.

(7) Mandal, B. P.; Kundu, M.; Bandyopadhyay, S. S. Physical solubility and diffusivity of N_2O and CO_2 into aqueous solutions of (2-amino-2-methyl-1-propanol + 20 monoethanolamine) and (N-methyldiethanolamine + monoethanolamine). *J. Chem. Eng. Data* **2005**, *50*, 352−358.

(8) Ebner, A. D.; Ritter, J. A. State-of-the-art adsorption and membrane separation processes for carbon dioxide production from carbon dioxide emitting industries. *Sep. Sci. Technol.* **2009**, *44*, 1273−1421.

(9) Serna-Guerrero, R.; Da'na, E.; Sayari, A. New insights into the interactions of CO_2 with amine-functionalized silica. *Ind. Eng. Chem. Res.* **2008**, *47*, 9406−9412.

(10) Keskin, S.; Sholl, D. S. Selecting metal organic frameworks as enabling materials in mixed matrix membranes for high efficiency natural gas purification. *Energy Environ. Sci.* **2010**, *3*, 343−351.

(11) Mason, J. A.; McDonald, T. M.; Bae, T. H.; Bachman, J. E.; Sumida, K.; Dutton, J. J.; Kaye, S. S.; Long, J. R. Application of a high-throughput analyzer in evaluating solid adsorbents for post-combustion carbon capture via multicomponent adsorption of CO_2, N_2, and H_2O. *J. Am. Chem. Soc.* **2015**, *137*, 4787−4803.

(12) Sumida, K.; Rogow, D. L.; Mason, J. A.; McDonald, T. M.; Bloch, E. D.; Herm, Z. R.; Bae, T. H.; Long, J. R. Carbon Dioxide Capture in Metal−Organic Frameworks. *J. R. Long, Chem. Rev.* **2012**, *112*, 724−781.

(13) Nugent, P.; Belmabkhout, Y.; Burd, S. D.; Cairns, A. J.; Luebke, R.; Forrest, K.; Pham, T.; Ma, S.; Space, B.; Wojtas, L.; Eddaoudi, M.; Zaworotko, M. J. Porous materials with optimal adsorption thermodynamics and kinetics for CO_2 separation. *Nature* **2013**, *495*, 80−84.

(14) Férey, G.; Mellot-Draznieks, C.; Serre, C.; Millange, F.; Dutour, J.; Surblé, S.; Margiolaki, I. *Science* **2005**, *309*, 2040−2042.

(15) Pal, A.; Chand, S.; Elahi, S. M.; Das, M. C. A microporous MOF with a polar pore surface exhibiting excellent selective adsorption of CO_2 from CO_2-N_2 and CO_2-CH_4 gas mixtures with high CO_2 loading. *Dalton T.* **2017**, *46*, 15280−15286.

(16) Torralba-Calleja, E.; Skinner, J.; Gutiérrez-Tauste, D. CO_2 capture in ionic liquids: a review of solubilities and experimental methods. *J. Chemother.* **2013**, *2013*, 1.

(17) Zhang, X.; Zhang, X.; Dong, H.; Zhao, Z.; Zhang, S.; Huang, Y. Carbon capture with ionic liquids: overview and progress. *Energy Environ. Sci.* **2012**, *5*, 6668−6681.

(18) Smith, E. L.; Abbott, A. P.; Ryder, K. S. Deep Eutectic Solvents (DESs) and their Applications. *Chem. Rev.* **2014**, *114*, 11060−11082.

(19) Ariyanto, T.; Masruroh, K.; Pambayun, G. Y. S.; Mukti, N. I. F.; Cahyono, R. B.; Prasetya, A.; Prasetyo, I. Improving the separation of CO_2/CH_4 using impregnation of deep eutectic solvents on porous Carbon. *ACS Omega* **2021**, *6*, 19194−19201.

(20) Dai, Y.; Van Spronsen, J.; Witkamp, G.; Verpoorte, R.; Choi, Y. H. Ionic liquids and deep eutectic solvents in natural products research: Mixtures of solids as extraction solvents. *Journal of Natural Product* **2013**, *76*, 2162−2173.

(21) Sarmad, S.; Mikkola, J. P.; Ji, X. Carbon dioxide capture with ionic liquids and deep eutectic solvents: A new generation of sorbents. *ChemSusChem* **2017**, *10*, 324−352.

(22) Li, X.; Hou, M.; Han, B.; Wang, X.; Zou, L. Solubility of CO_2 in a choline chloride + urea eutectic mixture. *J. Chem. Eng. Data* **2008**, *53*, 548−550.

(23) Leron, R. B.; Caparanga, A.; Li, M. H. Carbon dioxide solubility in a deep eutectic solvent based on choline chloride and urea at T = 303.15−343.15K and moderate pressures. *Journal of the Taiwan Institute of Chemical Engineers* **2013**, *44*, 879−885.

(24) Lin, H.; Gong, K.; Hykys, P.; Chen, D.; Ying, W.; Sofer, Z.; Yan, Y.; Li, Zh.; Peng, X. Nanoconfined deep eutectic solvent in laminated MXene for efficient CO_2 separation. *Chem. Eng. J.* **2021**, *405*, No. 126961.

(25) Ghazali, Z.; Hassan, N. H.; Yarmo, M. A.; Teh, L. P.; Othaman, R. Immobilization of Choline Chloride: Urea onto Mesoporous Silica for Carbon Dioxide Capture. *Sains Malaysiana* **2019**, *48* (5), 1025−1033.

(26) Endres, F.; Zein El Abedin, S. Air and water stable ionic liquids in physical chemistry. *Phys. Chem. Chem. Phys.* **2006**, *8*, 2101−2016.

(27) Noorani, N.; Mehrdad, A.; Ahadzadeh, I. CO2 absorption in amino acid-based ionic liquids: Experimental and theoretical studies. *Fluid Phase Equilib.* **2021**, *547*, No. 113185.

(28) Noorani, N.; Mehrdad, A.; Chakhmaghi, F. Thermodynamic study on carbon dioxide and methane permeability in polyvinyl-chloride/ionic liquid blends. *Chem. Thermodyn.* **2020**, *145*, No. 106094.

(29) Noorani, N.; Mehrdad, A. Modification of PVC with 1-vinylimidazole for CO_2/CH_4 separation: sorption, permeation and DFT studies. *Phys. Chem. Res.* **2020**, *8*, 689−703.

(30) Noorani, N.; Mehrdad, A. Cholinium-amino acid ionic liquids as biocompatible agents for carbon dioxide absorption. *J. Mol. Liq.* **2022**, *357*, No. 119078.
(31) Noorani, N.; Mehrdad, A.; Zarei diznab, R. Thermodynamic study on carbon dioxide absorption in vinyl imidazolium−amino acid ionic liquids. *Fluid Phase Equilib.* **2022**, *557*, No. 113433.
(32) Redlich, O.; Peterson, D. L. A useful adsorption isotherm. *J. Phys. Chem.* **1959**, *63*, 1024−1024.
(33) Yue, D. Y.; Jia, Y. Z.; Yao, Y.; Sun, J. H.; Jing, Y. Structure and electrochemical behavior of ionic liquid analogue based on choline chloride and urea. *Electrochim. Acta* **2012**, *65*, 30−36.
(34) Delgado-Mellado, N.; Larriba, M.; Navarro, P.; Rigual, V.; Ayuso, M.; García, J.; Rodríguez, F. Thermal stability of choline chloride deep eutectic solvents by TGA/FTIR−ATR analysis. *J. Mol. Liq.* **2018**, *260*, 37−43.
(35) Vu, T. A.; Le, G. H.; Dao, C. D.; Dang, L.; Nguyen, K. T.; Dang, P. T.; Tran, H. T. K.; Duong, Q. T.; Nguyen, T. V.; Lee, G. D. Isomorphous substitution of Cr by Fe in MIL-101 framework and its application as a novel heterogeneous photo-Fenton catalyst for reactive dye degradation. *RSC Adv.* **2014**, *4*, 41185−41194.
(36) Wang, J.; Yang, M.; Dong, W.; Jin, Z.; Tang, J.; Fan, S.; Lu, Y.; Wang, G. Co(ii) complexes loaded into metal−organic frameworks as efficient heterogeneous catalysts for aerobic epoxidation of olefins. *Catalysis Science & Technology* **2016**, *6*, 161−168.
(37) Rouquerol, J.; Rouquerol, F.; Llewellyn, P.; Maurin, G.; Sing, K. S. W. *Adsorption by Powders and Porous Solids*; 2nd Ed., Academic Press: London, 2013.
(38) Kim, J.; Kim, W. Y.; Ahn, W. S. Amine-functionalized MIL-53(Al) for CO_2/N_2 separation: Effect of textural properties. *Fuel* **2012**, *102*, 574−579.
(39) Chen, X. Y.; Hoang, V. T.; Rodrigue, D.; Kaliaguine, S. Optimization of continuous phase in amino-functionalized metal-organic framework (MIL-53) based co-polyimide mixed matrix membranes for CO2/CH4 separation. *RSC Adv.* **2013**, *3*, 24266−24279.
(40) Su, W. C.; Wong, D. S. H.; Li, M. H. Effect of water on solubility of carbon dioxide in (aminomethanamide + 2-hydroxy-n,n,n-trimethylethanaminium chloride). *J. Chem. Eng. Data* **2009**, *54*, 1951−1955.
(41) Lawson, S.; Griffin, C.; Rapp, K.; Rownaghi, A. A.; Rezaei, F. Amine-functionalized MIL-101 monoliths for CO_2 removal from enclosed environments. *Energy Fuels* **2019**, *33*, 2399−2407.
(42) Kenarsari, S. D.; Yang, D.; Jiang, G.; Zhang, S.; Wang, J.; Russell, A. G.; Wei, Q.; Fan, M. Review of Recent Advances in Carbon Dioxide Separation and Capture. *RSC Adv.* **2013**, *3*, 22739−22773.
(43) Builes, S.; Sandler, S. I.; Xiong, R. Isosteric Heats of Gas and Liquid Adsorption. *Langmuir* **2013**, *29*, 10416−10422.
(44) Sircar, S.; Mohr, R.; Ristic, C.; Rao, M. B. Isosteric Heat of Adsorption: Theory and Experiment. *J. Phys. Chem. B* **1999**, *103*, 6539−6546.
(45) Marathe, R. P.; Farooq, S.; Srinivasan, M. P. Modeling Gas Adsorption and Transport in Small-Pore Titanium Silicates. *Langmuir* **2005**, *21*, 4532−4546.
(46) Pourebrahimi, S.; Kazemeini, M.; Ganji Babakhani, E.; Taheri, A. Removal of the CO_2 from flue gas utilizing hybrid composite adsorbent MIL-53(Al)/GNP metal-organic framework. *Microporous Mesoporous Mater.* **2015**, *218*, 144−152.
(47) Frisch, M. J.; Trucks, G. W.; Schlegel, H. B.; Scuseria, G. E.; Robb, M. A.; Cheeseman, J. R.; Montgomery, J. A.; Vreven, T.; Kudin, K. N.; Burant, J. C.; Millam, J. M.; Iyengar, S. S.; Tomasi, J.; Barone, V.; Mennucci, B.; Cossi, M.; Scalmani, G.; Rega, N.; Petersson, G. A.; Nakatsuji, H.; Hada, M.; Ehara, M.; Toyota, K.; Fukuda, R.; Hasegawa, J.; Ishida, M.; Nakajima, T.; Honda, Y.; Kitao, O.; Nakai, H.; Klene, M.; Li, X.; Knox, J. E.; Hratchian, H. P.; Cross, J. B.; Bakken, V.; Adamo, C.; Jaramillo, J.; Gomperts, R.; Stratmann, R. E.; Yazyev, O.; Austin, A. J.; Cammi, R.; Pomelli, C.; Ochterski, J. W.; Ayala, P. Y.; Morokuma, K.; Voth, G. A.; Salvador, P.; Dannenberg, J. J.; Zakrzewski, V. G.; Dapprich, S.; Daniels, A. D.; Strain, M. C.; Farkas, O.; Malick, D. K.; Rabuck, A. D.; Raghavachari, K.; Foresman, J. B.; Ortiz, J. V.; Cui, Q.; Baboul, A. G.; Clifford, S.; Cioslowski, J.; Stefanov, B. B.; Liu, G.; Liashenko, A.; Piskorz, P.; Komaromi, I.; R, L.; Martin, D. J.; Fox, T.; Keith, A.; Laham, C. Y.; Peng, A.; Nanayakkara, M.; Challacombe Gill, P. M. W.; Johnson, B.; Chen, W.; Wong, M. W.; Gonzalez, C.; Pople, J. A. *Gaussian 03. Revision B.03*. Gaussian, Inc., Pittsburgh, 2003.
(48) Becke, A. D. Density-functional thermochemistry. III. The role of exact exchange. *J. Chem. Phys.* **1993**, *98*, 5648−5652.
(49) Lee, C.; Yang, W.; Parr, R. G. Development of the Colle−Salvetti correlation-energy formula into a functional of the electron density. *Phys. Rev. B* **1988**, *37*, 785−789.
(50) Mehrdad, A.; Noorani, N. Permeability behavior of polyvinyl chloride-ionic liquid ionomer for CO_2/CH_4 separation. *Sep. Purif. Technol.* **2019**, *226*, 138−145.

https://doi.org/10.1021/acsomega.3c09243
ACS Omega 2024, 9, 9516−9525